Surface Plasmon-Coupled Emission and Fabry−Perot Resonance in the Sample Layer: A Theoretical Approach

Nils Calander*

Department of Physics, Chalmers University of Technology, SE-412 96 Göteborg, Sweden

Received: March 2, 2005; In Final Form: May 25, 2005

A theoretical approach is used to investigate the coupling of surface plasmon-coupled emission to Fabry−Perot resonance in the sample layer. Quantities investigated are emission angles, polarization, power levels, and fluorescence lifetimes. The results are compared to experimental findings. For comparison a layered structure without surface plasmons, possessing only dielectric Fabry−Perot resonances, is explored. This structure seems to be amenable to s-polarization only but is in principle loss-less and has more degrees of freedom for design and optimization.

Introduction

Fluorescence spectroscopy is of widespread use for high-sensitivity detection and analysis in many fields of biotechnology. Resonance enhancement of the fluorescence signal is a way of improving the sensitivity and selectivity. Surface plasmon resonance (SPR) is used for this purpose. Surface plasmon-coupled emission (SPCE) has been treated in a number of recent articles[1−14] and has shown promises for concentration of the emission to specific angles and polarizations which make it easily collected. In a recent article[12] the effect of the sample thickness, i.e., a dielectric layer possessing resonances containing the sample fluorophores, on the optical properties of the SPCE has been experimentally investigated. This topic is explored here theoretically, and experimental results in ref 12 are explained and at the same time the theoretical approach in ref 14 is reinforced. The surface plasmon resonances are coupled together with the resonances in the sample layer, which is basically a Fabry−Perot interferometer, i.e., two mirrors with a dielectric medium in between. One mirror is due to the silver layer and the other to internal reflections at the interface of the sample layer to air.

For comparison, the theoretical approach is also used in a different setup without the use of a silver layer, and therefore without surface plasmons. In this approach the silver layer (mirror) is replaced by an alternating dielectric mirror. This kind of low-loss semitransparent mirror is often used for creating laser resonators. It is found that this approach should be well-suited for directing emission from fluorophores in specific directions. It seems though that mostly s-polarized emission is obtained in this way.

Basic Theory

The theoretical method used is described in the Supporting Information section. The method uses that the radiation from a dipole can be decomposed into an integral over plane waves, which is a two-dimensional Fourier transform. The decomposition is also called the Weyl identity. Fresnel theory, i.e., the theory of refraction of plane waves in a dielectric planar structure, can then be applied to the plane waves individually.

* E-mail: nils.calander@fy.chalmers.se.

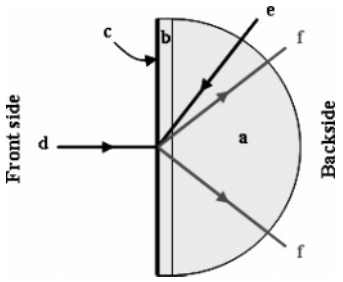

Figure 1. Basic experimental setup: (a) hemispherical glass prism; (b) microscope glass slide index-glued to the prism; (c) the resonance and fluorophore-containing layers; (d) excitation light in the reverse Kretschmann (RK) configuration ($\lambda = 514$ nm); (e) excitation light in the Kretschmann (KR) configuration ($\lambda = 514$ nm); (f) emission light to be detected (600 nm).

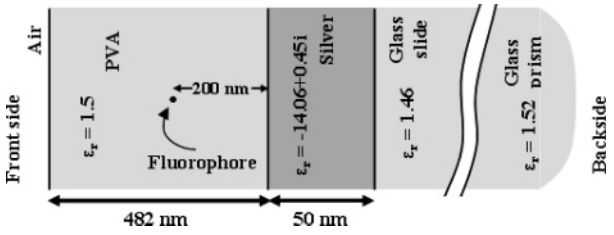

Figure 2. Geometry and dielectric constants of the structure in Figure 1c. Excitation wavelength = 514 nm; emission wavelength = 600 nm.

Simulations of SPCE at Planar Fabry−Perot Structures

The basic overall structure studied is the same as that in ref 12 and is shown in Figure 1. A microscope glass slide is index-glued to a hemispherical glass prism. The resonance layers (surface plasmon and Fabry−Perot) are deposited onto the glass slide, i.e., a silver layer of 50 nm thickness and a PVA (poly(vinyl alcohol)) layer containing the fluorophores (sulforhodamine 101). Excitation light is coming either from the front side (reverse Kretschmann configuration, RK) or from the backside (Kretschmann configuration, KR). Emission light is concentrated at specific angles and polarizations and is collected at the backside. The excitation light has the wavelength 514 nm and the emission around 600 nm. The details of the layered structure in Figure 1 at c are shown in Figure 2.

10.1021/jp0510544 CCC: $30.25
Published on Web 06/28/2005

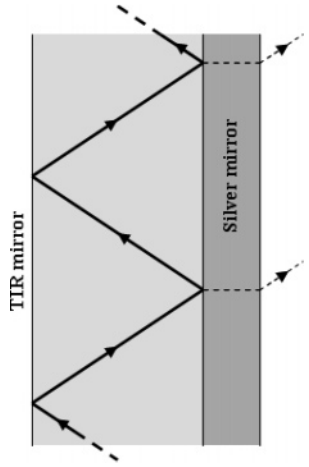

Figure 3. The PVA layer acts as a Fabry−Perot interferometer. Internal reflection at the PVA−air interface constitutes the left mirror. Beyond a critical angle there is total internal reflection (TIR); otherwise the reflection is partial. At the right is a silver mirror. Since the conditions for reflection are different at different polarizations, radiation peaks with different polarization show up in Figure 4. The resonance modes in the Fabry−Perot interferometer interact with the surface plasmon resonances in the silver layer. For the electric field from a fluorophore in this structure, see Figure 5.

The silver layer possesses surface plasmon resonances. The PVA layer is acting as a Fabry−Perot interferometer, which is illustrated in Figure 3. The surface plasmon resonances and the Fabry−Perot resonances act together if polarization is suitable. For s-polarization only Fabry−Perot resonances occur, while for p-polarization hybrid surface plasmon−Fabry−Perot resonances occur. The emission from the fluorophores is affected by these resonances and appears at the backside at specific angles. The calculated emission diagrams are shown in Figure 4. For fluorophores with dipoles in parallel to the planar structures, both s- and p-polarization appear in the emission light at different angles. For fluorophores with dipoles perpendicular to the planar structures, only p-polarized light appears. The phase change of reflected light at the "Fabry−Perot mirrors" depends on the polarization, which explains why the peaks for the s- and p-polarizations occur at different angles. In Figure 4d the emission from a fluorophore oriented parallel to the planes is seen from the backside. This shows the variation of the emitted light in azimuth, and the figure should be compared to Figures 3 and 5 in ref 12 and Figure 4 in ref 14. Emission occurs in concentric semicircles with alternating s- and p-polarizations. The behavior is explained in Figure 3 in terms of Fabry−Perot resonances.

In Figure 5 the electromagnetic near field is shown. Spread-out near field in Figure 5 corresponds to narrow far-field peaks in Figure 4 and vice versa. Parts a and b of Figure 5 show the near field from a dipole oriented such that only s-polarization occurs in the figure. There are no surface plasmon resonances. The near field is spread out and the corresponding far-field peaks narrow as is seen in Figure 4b. Parts c and d of Figure 5 show the near field from a dipole oriented such that only p-polarization occurs in the figure. Hybrid surface plasmon−Fabry−Perot

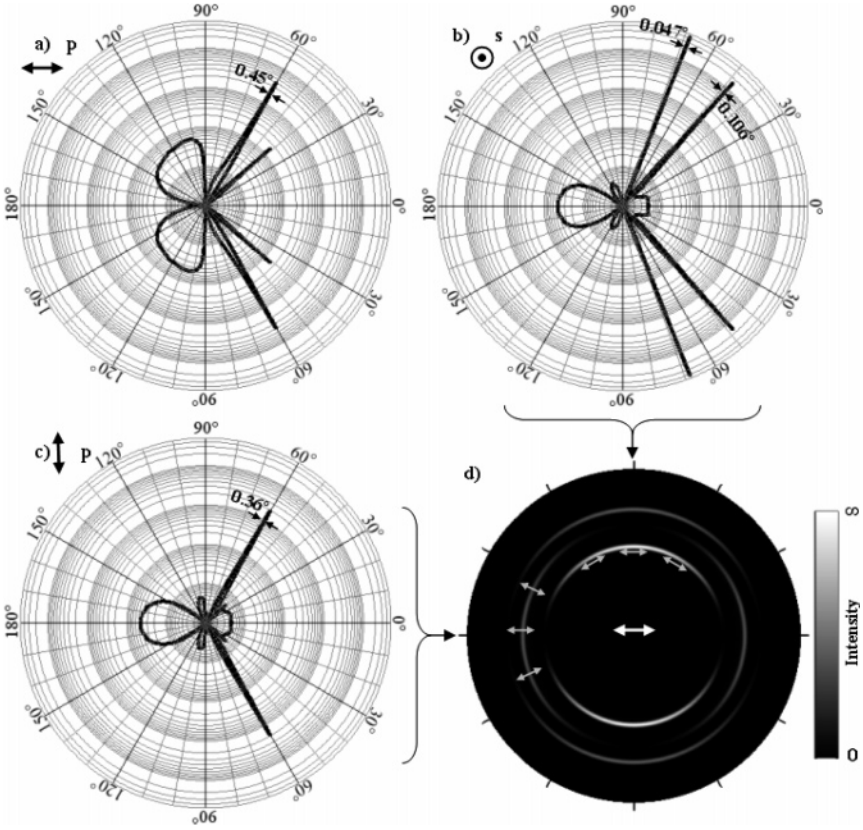

Figure 4. Far field intensities: (a−c) Radiation diagrams from a fluorophore as in Figure 2. They show power per steradian. The total power from a fluorophore in infinite homogeneous PVA is normalized to one. Fluorophore transition moment orientation is indicated by the arrows. Polarization is indicated by the letters. The indicated widths are full widths at half-maximum (fwhm). A real fluorophore emits with a finite bandwidth, which means that the peaks in reality are wider because the peak angles depend on wavelength. (d) Radiation intensity as seen on a projection screen at the backside. Since some of the peaks are rather narrow, the resolution of this plot is not high enough to show the correct intensities of the respective peaks. The power of the p-peak is higher than the power from the s-peaks at this particular position of the fluorophore. This is not always the case; see Figure 8. The orientation of the fluorophore transition moment is indicated by the arrow in the middle and the polarization by the small gray arrows. Correspondence between b, c, and d is indicated.

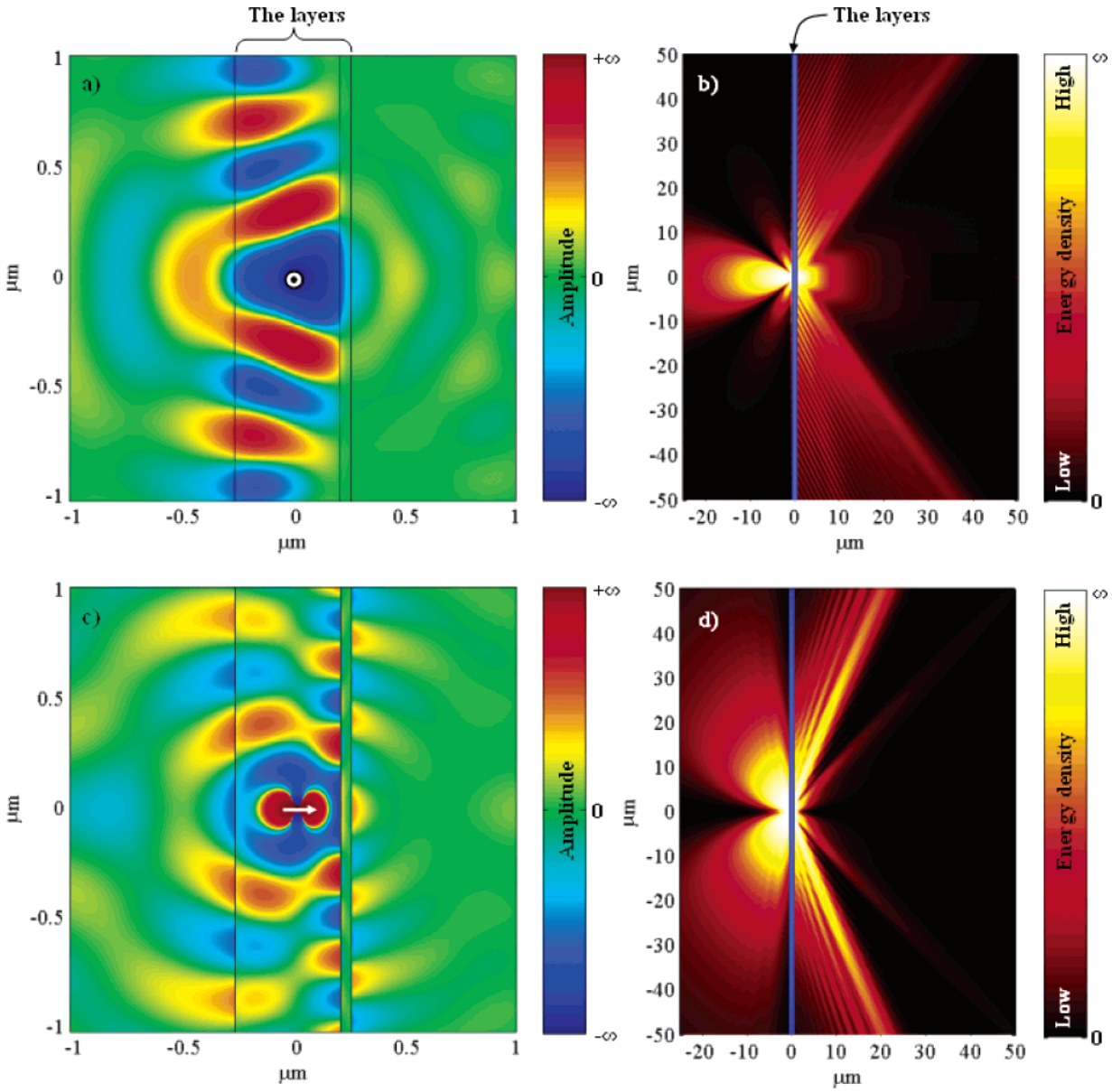

Figure 5. Plots of the near field in a plane through the oscillating dipole placed and oriented as indicated. (a) The electric field, which in this case only has a component parallel to the dipole, at a specific instant of time. It has only Fabry−Perot character and is mainly concentrated to the PVA layer. (b) The energy density from a dipole placed and oriented as in a. Note that the narrow peaks for the far field in Figure 4b correspond to spread-out radiation at the near field. (c) The electric field component parallel to the dipole. A typical surface plasmon field pattern at the silver layer appears. (d) The energy density from a dipole placed and oriented as in c. Note that the near field is not as spread out and that the corresponding far field in Figure 4a is not as narrow. This is due to the higher losses (resistive or radiative) in surface plasmon modes such that they reach less far out in the plane from the fluorophore.

resonance modes show up. The near field is not as spread out and the corresponding farfield peak in Figure 4a not as narrow. This seems to be due to that the surface plasmon resonances have more loss. This loss may either be resistive loss in the silver layer or radiative output to the SPCE. The field in the layers is therefore more localized near the fluorophore since the surface plasmons lose more energy when propagating in the layer.

Figure 6 shows the total power radiated into the two main directions. The power is normalized to the power radiated from a fluorophore in an infinite homogeneous medium of the same refractive index. As seen, a large part of the power is dissipated in the silver layer. In a different layered structure, without silver, investigated in the next section of this article, this problem is circumvented by use of loss-less materials.

The radiated output power depends on the position of the fluorophore in the PVA layer as illustrated in Figure 7. Typical "wavy" higher-order resonance mode patterns are evident. It is also seen that the power flow between the fluorophore and the silver increases near the silver. Most of this increased power is dissipated in the silver layer. The perpendicular dipole shows the strongest increase. This is due to that it excites more p-polarized surface plasmons, some of which create the SPCE. The resistive power dissipation causes a shortening of lifetime without raising the output power.

In Figure 8 the output power at the respective peak is plotted versus the fluorophore position for the sample layer thickness of 482 nm. As is seen the different peaks correspond to different resonance modes in the PVA layer, with different numbers of maxima and minima.

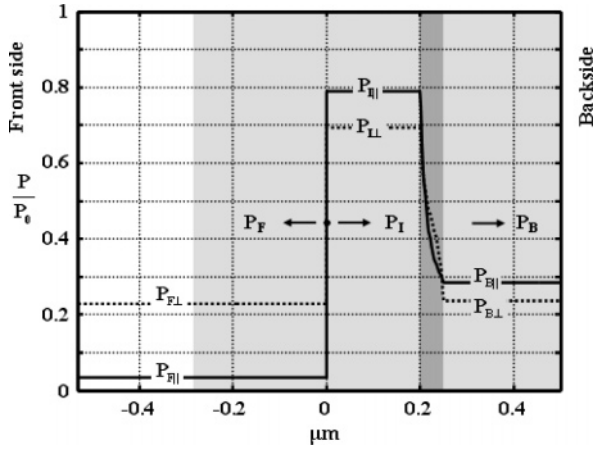

Figure 6. Power flow through the respective layers. The || indicates that the fluorophore is oriented parallel to the layers, and ⊥, that it is oriented perpendicular. The power is normalized to the total power radiating from a fluorophore in a homogeneous medium with the same refractive index. P_B is the power into the backside, P_F into the frontside, and P_I in the region between the fluorophore and the silver.

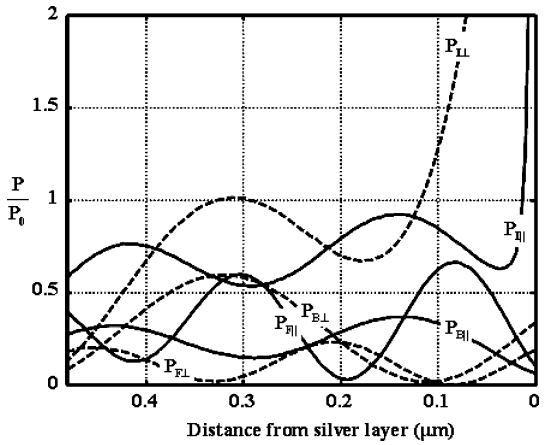

Figure 7. Total normalized power from the fluorophore versus distance from the silver layer. The power flow is at the backside ($P_{B\perp}$ and $P_{B\parallel}$), between the fluorophore and the silver layer ($P_{\perp\perp}$ and $P_{\parallel\parallel}$), and at the front side ($P_{F\perp}$ and $P_{F\parallel}$). For power notations, see Figure 6. The sample layer thickness is in this case 482 nm. Note that the power flow between the fluorophore and the silver rises steeply near the silver layer, especially for the dipole perpendicular to the planar structure. This is due to higher excitation and dissipation of surface plasmons.

In Figure 9 the standing waves of the square of the electric field from the excitation light (wavelength = 514 nm) is plotted versus position in the sample layer. The excitation light is from either the Kretschmann or reverse Kretschmann configuration. Resonance mode structures with maxima and minima are seen. In an experimental situation the excitation is important for the final emission and should be weighted in for a faithful simulation. This weighting has been done in Table 1.

Calculated values of angles, intensities, lifetimes, efficiencies, and losses are shown in Table 1. Experimental values of angles and intensities from ref 12 are also shown. The intensities are normalized to the largest peak. The lifetimes are averages at the respective peaks and normalized to the lifetime of a fluorophore in an infinite homogeneous medium with the same properties as the sample layer. The efficiency η is here the total power radiated into the backside divided by the total power radiated by the fluorophores. The loss is the power dissipated in the silver layer divided by the total power radiated by the fluorophores.

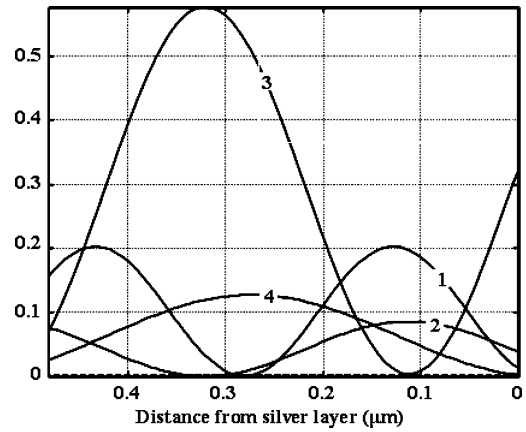

Figure 8. Contribution to the output power at the respective peaks from a fluorophore at various positions and orientations in the sample layer: 1, || 48.2; 2, || 60.0; 3, ⊥ 60.0; 4, || 68.3.

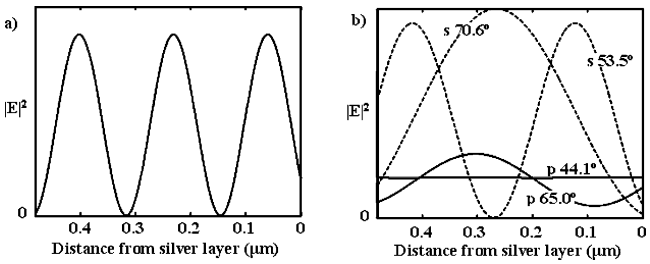

Figure 9. Standing wave pattern, i.e., the excitation electric field squared in the sample layer of thickness 482 nm. The excitation light is polarized parallel to the plane and is coming from the front side at normal incidence (RK) in a. The excitation light is coming from the backside at the respective angles where resonance appear (KR) in b. The excitation wavelength is 514 nm. The permittivity of the silver layer at this wavelength is assumed to be $\epsilon_r = -9 + 0.3i$ (from ref 12).

The small discrepancies of the experimental and theoretical angles may be due to inaccuracies in the sample layer thicknesses and refractive indices. Calculations show that there should also be a fifth peak at the 745 nm PVA layer which is not listed experimentally. It is s-polarized at 73.6° and has very low intensity.

In the calculations of intensities, lifetimes, efficiencies, and losses a number of different distributions of the fluorophore positions and orientations, and different degrees of saturation of the fluorophores, have been tested. The fluorophores are assumed to be excited by short pulses (120 ps half-width which is much shorter than the lifetimes of about 2−3 ns [12]). If saturation occurs, the fluorophores are assumed to always become excited. If saturation does not occur the probability of excitation depends on the square of the component of the local electric field parallel to the dipole. Far from saturation the probability of excitation is proportional to the square of that component of the electric field. The exciting field is assumed to come at normal incidence at the reverse Kretschmann configuration. The time period between the exciting pulses is assumed long enough such that an excited fluorophore emits a photon (the pulse repetition frequency is 76 MHz, which means 13 ns between pulses, which is much longer than the lifetimes of 2−3 ns [12]).

The calculated values shown in Table 1 are for fluorophores uniformly distributed within the layer but with a distribution of directions exaggerated normal to the planar structure. The angular distribution is assumed proportional to $\cos^4\theta$, where θ is the angle between the fluorophore dipole and the normal of the planar structure. The fluorophores are assumed far from

TABLE 1: Calculated Values Together with Experimental from Ref 1[a]

d (nm)	polarization	Θ (deg) (exp)	Θ (deg) (theor)	I_{REL} (exp)	I_{REL} (theor)	⟨τ⟩ (theor)	η (theor)	loss (theor)
37	p	50.0	50.0	1.00	1.00	0.87	0.35	0.55
70	p	62.5	62.0	1.00	1.00	0.60	0.40	0.48
156	s	46.5	45.6	1.00	1.00	0.67	0.08	0.83
290	p	43.75	44.1	1.00	1.00	1.41	0.11	0.73
	s	60.0	59.3	0.78	0.75	1.43		
482	s	45.5	48.2	0.30	0.32	1.48		
	p	58.0	60.0	1.00	1.00	1.33	0.20	0.61
	s	70.25	68.3	0.12	0.22	1.50		
745	s	44.5	46.1	0.27	0.27	1.55		
	p	52.5	53.9	1.00	0.82	1.57		
	s	62.0	60.9	0.22	0.26	1.66	0.22	0.55
	p	70.75	70.0	0.11	1.00	1.60		
	s	−	73.6	−	0.05	1.66		

[a] The intensity I_{REL} at the respective peaks is normalized to the most intense peak. The theoretical values are averages over position and orientation of the fluorophores (weighted distributions, in orientation as $\cos^4\theta$) as described in the text. The fluorophores are assumed not to be saturated by the excitation. The average of the fluorescence lifetimes ⟨τ⟩ are for the same distributions. The lifetimes are normalized to the lifetime in a homogeneous medium with the same properties as the PVA layer. Note the trend of shorter lifetimes for thinner PVA layer but with some modification due to resonance phenomena. The lifetimes are slightly smaller than one for the thinner PVA layers and slightly larger than one for the thicker. The efficiency is the output power to the backside divided by the total output power from the fluorophores. The loss is the power dissipated in the silver layer divided by the total output power from the fluorophores.

saturation by the exciting light pulses. As is seen in the table the relative experimental intensities of the respective peaks are at least qualitatively described by the theoretical calculations except for the p-polarized peak at 70° for the 745 nm thick PVA layer, where the theoretical value is much larger than the experimental one. By testing it seems like concentration of the fluorophores near the surfaces would make that peak lower but not enough to match the experimental value. The distribution of fluorophores in position and orientation and the degree of saturation chosen do not have to be the ones with the closest fit to the experimental intensities.

The lifetimes seem to be shorter for thinner PVA layers. That is consistent with more quenching of the fluorophores near the silver layer. The lifetime for the thinnest layer is somewhat longer than for the next thinnest, which may be due to resonance effects. Generally, the efficiencies are low and the losses of the excited light in the silver layer high. The emission angles are seen to be almost independent of fluorophore position and orientation.

The fluorescence lifetime is inversely proportional to the total power from the fluorophore. The average of the lifetimes in Table 1 is over all possible orientations and positions in the PVA layer, weighted by the $\cos^4\theta$ distribution in orientation and by the probability of excitation which is proportional to the square of the excitation electric field component along the dipole. The average lifetimes seen at the respective peaks are also weighted by the relative output powers for the peaks.

As noted in ref 14 a thinner silver layer may dissipate less of the dipolar output. It is also the case with the thicker PVA layers studied in this article. Figure 6 in ref 14 looks very similar even if the PVA layer is thick, but the fluorophore still has to be close to the silver. Also in the thick PVA layer case the SPCE peaks (p-polarized) are wider for thinner silver layers so there is still a compromise between output power and peak sharpness. This widening is partly due to the higher resistive losses and partly to the higher radiative outputs (SPCE), which causes a localization of the nearfield. The s-polarized output is also widened, but less than the p-polarized output.

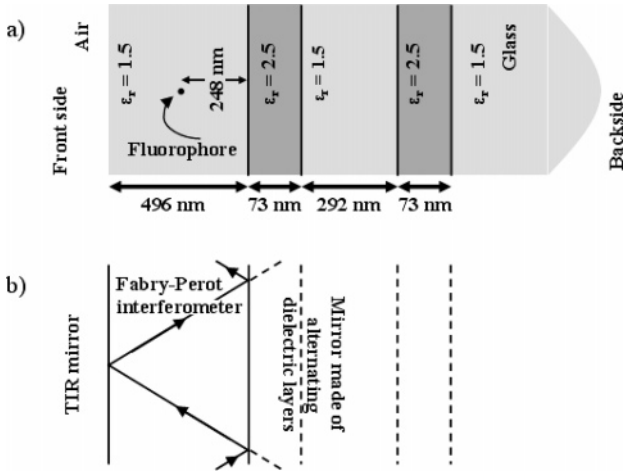

Figure 10. (a) Geometry and dielectric constants used in the calculations. All layers are purely dielectric, without losses. (b) The leftmost layer is designed to have an s-polarized waveguide resonance due to reflections of a plane wave at 70°, at the front side due to total internal reflection (TIR) and at the other side due to the (semitransparent) mirror of alternating quarter wave layers of alternating refractive indices. The same resonance mode also exists in Figures 2 and 3, but with a silver mirror.

One may think that matching the surface plasmon resonance in the silver layer with a resonant mode in the Fabry−Perot PVA layer will strongly enhance the SPCE. It indeed seems like the p-polarized resonant peaks, especially widths but also intensities, are critically dependent on the respective layer thicknesses, which should then reflect this matching. The problem seems to be rather involved though since the surface plasmon resonance is dependent on the Fabry−Perot resonator properties.

In conclusion of the simulation of the experimentally investigated structure it seems that the experimental values in most cases can be reproduced theoretically by assuming suitable distributions in position and orientation and by assuming a suitable state of saturation of the fluorophores by the excitation light pulses.

Simulation of Fluorescence in Fabry−Perot Structures with Purely Dielectric Mirrors

A theoretical comparison is here done with a different setup, without the use of a metallic layer and surface plasmon resonance. It is replaced by a dielectric layered structure of alternating refractive indices. High refractive index layers[15−18] could be made of, for example, lithium niobate ($LiNbO_3$) with a refractive index of 2.3 at the optical wavelength used here, or composites of polymeric materials and metal sulfides or heavy-metal oxides (refractive indices for poly(ethylene oxide)/FeS_2 are 2.5−2.8).

The basic layered structure is illustrated in Figure 10. The mirrors of the Fabry−Perot interferometer are now entirely dielectric. The left mirror is due to internal reflection or total internal reflection as before. The silver mirror at the right is replaced by a semitransparent mirror of alternating layers of high and low refractive indices. The mirror is loss-less and can be designed to suit any angle and semitransparency.

Figure 11a shows the emission diagram for a fluorophore with radiating dipole parallel to the planar structure. Compare this diagram with Figure 4b. The emission is s-polarized.

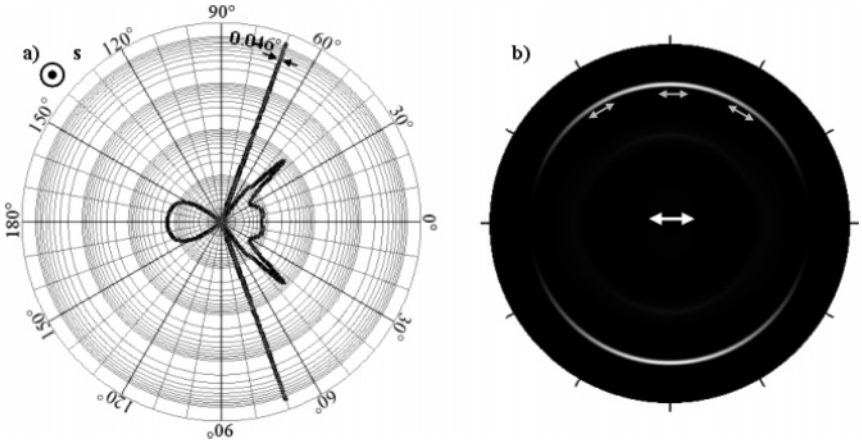

Figure 11. (a) Radiation diagram from a fluorophore as in Figure 10a. It shows power per steradian as in Figure 4a−c. The narrow peak at 70° has about 58% of the power of the radiation to the backside. (b) Radiation intensity as seen on a projection screen at the backside. The orientation of the fluorophore transition moment is indicated by the arrow in the middle and the polarization by the small gray arrows.

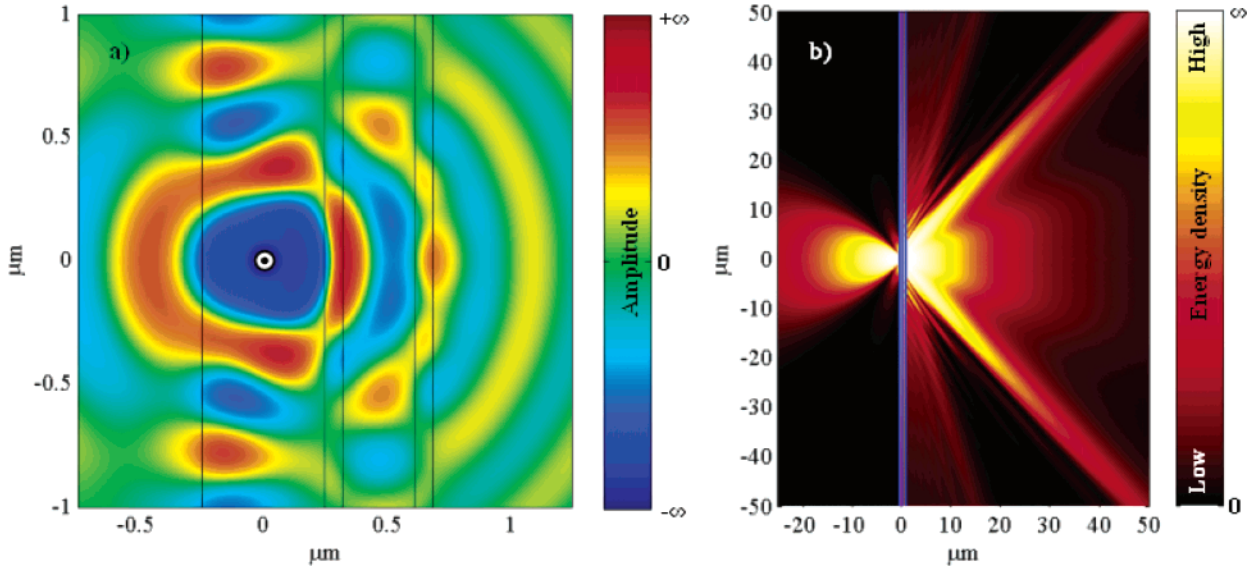

Figure 12. Plots of the near field in a plane through the oscillating dipole placed and oriented as indicated: (a) electric field, which only has a component parallel to the dipole, at a specific instant of time; (b) energy density. Note that the narrow peak at 70° for the far field in Figure 11a corresponds to spread-out radiation at the near field, and the wider peak at 45° for the far field corresponds to rather collected near field which then looks brighter in the figure.

Because of difficulties in designing good mirror properties for p-polarized light using alternating dielectric layers, there is almost no counterpart to Figure 4c. Therefore the diagram in Figure 11a lacks p-polarized semicircles, which are present in Figure 4d. A component of the near-field and the energy density are shown in Figure 12. The narrow and wide peaks in Figure 11a have roughly the same power. The narrow peak in Figure 11a shows a much more spread-out energy density in Figure 12b than the wide peak does, due to Fourier reasons, and therefore does not appear as dense.

The total radiated power in either direction is shown in Figure 13. There is no loss in any layer making the output power to the right much higher than in the silver case (Figure 6).

Finally, the position of the fluorophore in the PVA layer is of importance to the output power, as is seen in Figure 14; compare Figure 7.

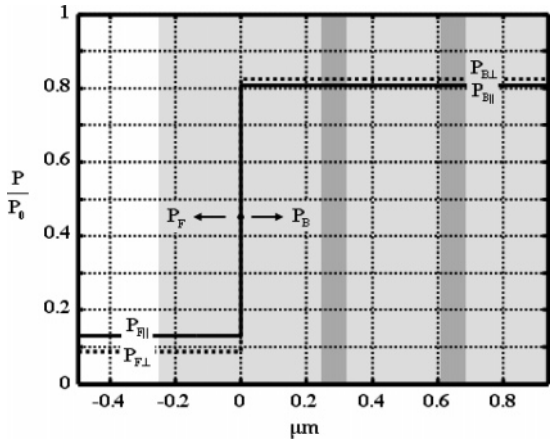

Figure 13. Power flow through the respective layers. The || indicates that the fluorophore is oriented in parallel to the layers, and ⊥, that it is oriented perpendicular. The power is normalized to the total power radiating from a fluorophore in an infinite homogeneous medium with the same refractive index. Note that there are no losses here. In Figure 6 there are losses in the silver layer.

Conclusions

The theoretical approach developed in ref 14 has been used to simulate the experiments in ref 12. Surface plasmon resonances in a silver layer are coupled to waveguide (Fabry−

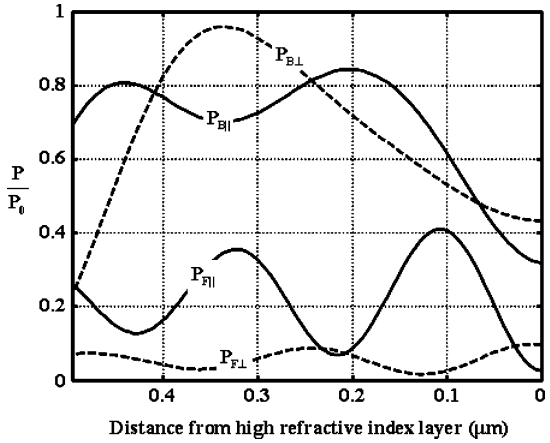

Figure 14. Corresponding to Figure 7. Because the mediums are lossless in this case, the P_I and P_B powers are the same.

Perot) modes in a dielectric layer containing the fluorophores if polarization is suitable, i.e., p-polarization. Only Fabry−Perot resonance modes show up for s-polarization. The correctness of the theory has been reinforced. Additionally, a different layered structure without surface plasmons has been simulated and compared to the first simulation. In this case only waveguide (Fabry−Perot) modes are present and show similar behavior for the s-polarized wave. No p-polarized emission exists. There are in principle no losses in this case, and the structure is more amenable (more degrees of freedom) to design at different wavelengths and emission angles.

As is noted in ref 12, the existence of SPCE related to waveguide modes should offer numerous advantages for both the study of SPCE itself and for its use in sensing devices. The alternative structure should also find its use in sensing devices.

Since the angles and polarization are strongly dependent on the thickness and optical properties of the sample layer, this should allow determination of its thickness and optical properties. This could be applied to for example highly oriented systems such as lipid bilayers and Langmuir−Blodgett films. Also, as indicated in this article, an analyte distribution in the sample layer could be elucidated. The structure should make examination without movable parts possible, allowing development of portable devices.

Supporting Information Available: A derivation of the equations used for the electromagnetic calculations is available as Supporting Information. This material is available free of charge via the Internet at http://pubs.acs.org.

References and Notes

(1) Lakowicz, J. R. *Anal. Biochem.* **2004**, *324*, 153.
(2) Malicka, J.; Gryczynski, I.; Gryczynski, Z.; Lakowicz, J. R. *J. Phys. Chem. B* **2004**, *108*, 19114.
(3) Malicka, J.; Gryczynski, I.; Gryczynski, Z.; Lakowicz, J. R. *J. Biomol. Screening* **2004**, *9*, 208.
(4) Matveeva, E.; Gryczynski, Z.; Gryczynski, I.; Malicka, J.; Lakowicz, J. R. *Anal. Chem.* **2004**, *76*, 6287.
(5) Matveeva, E.; Gryczynski, Z.; Gryczynski, I.; Lakowicz, J. R. *J. Immunol. Methods* **2004**, *286*, 133.
(6) Matveeva, E.; Malicka, J.; Gryczynski, I.; Gryczynski, Z.; Lakowicz, J. R. *Biochem. Biophys. Res. Commun.* **2004**, *313*, 721.
(7) Zhang, J.; Gryczynski, Z.; Lakowicz, J. R. *Chem. Phys. Lett.* **2004**, *393*, 483.
(8) Gryczynski, I.; Malicka, J.; Gryczynski, Z.; Lakowicz, J. R. *Anal. Biochem.* **2004**, *324*, 170.
(9) Gryczynski, Z.; Malicka, J.; Matveeva, E.; Gryczynski, I.; Lakowicz, J. R. *Biophys. J.* **2004**, *86*, 359A.
(10) Gryczynski, I.; Malicka, J.; Gryczynski, Z.; Nowaczyk, K.; Lakowicz, J. R. *Anal. Chem.* **2004**, *76*, 4076.
(11) Gryczynski, I.; Malicka, J.; Gryczynski, Z.; Lakowicz, J. R. *J. Phys. Chem. B* **2004**, *108*, 12568.
(12) Gryczynski, I.; Malicka, J.; Nowaczyk, K.; Gryczynski, Z.; Lakowicz, J. R. *J. Phys. Chem. B* **2004**, *108*, 12073.
(13) Geddes, C. D.; Gryczynski, I.; Malicka, J.; Gryczynski, Z.; Lakowicz, J. R. *J. Fluoresc.* **2004**, *14*, 119.
(14) Calander, N. *Anal. Chem.* **2004**, *76*, 2168.
(15) Ajo-Franklin, C. M.; Kam, L.; Boxer, S. G. *Proc. Natl. Acad. Sci. U. S. A.* **2001**, *98*, 13643.
(16) Caseri, W. *Macromol. Rapid Commun.* **2000**, *21*, 705.
(17) KyprianidouLeodidou, T.; Althaus, H. J.; Wyser, Y.; Vetter, D.; Buchler, M.; Caseri, W.; Suter, U. W. *J. Mater. Res.* **1997**, *12*, 2198.
(18) Sanz, O.; Gonzalo, J.; Perea, A.; Fernandez-Navarro, J. M.; Afonso, C. N.; Lopez, J. G. *Appl. Phys. A: Mater. Sci. Process.* **2004**, *79*, 1907.